Peer-reviewed version available at Actuators 2019, 8, 58; doi:10.3390/act8030058

Article

Soft driving epicyclical mechanism for robotic finger

Jose Ramirez *, Astrid Rubiano and Paola Castiblanco

Universidad Militar Nueva Granada, 250547 Cajicá, Km 2 de la vía Cajicá-Zipaquirá, CO
u3900255@unimilitar.edu.co (P.C.); astrid.rubiano@unimilitar.edu.co (A.R.); jose.ramirez@unimilitar.edu.co (J.R.)
* Correspondence: jose.ramirez@unimilitar.edu.co; Tel.: +57-315-4549665

Abstract: Nowadays, the development or improvement of actuation mechanisms is a crucial topic for the achievement of dextrous manipulation using soft robots. Then, a primary target of research is the design of actuation and driving devices. Consequently, in this paper, we introduce a soft driving epicyclical mechanism that mimics human muscle behavior and fulfills motion requirements to achieve grasping gestures using a robotic finger. The prototype is experimentally assessed, and results show that our approach has enough performance for the implementation in grasping tasks. Furthermore, we introduce the basis for a new soft epicyclical mechanism merger with shape memory alloys to allow active stiffness control of the mechanism.

Keywords: Actuation and driving mechanism; soft robotics; soft epicyclical mechanism; Shape Memory Alloy

1. Introduction

The task of designing or improving a robotic hand (to replicate the grasping capabilities and the kinematic functionality of the human hand) involves the consideration of a high complexity sensory and motor functions. The literature (*e.g.* [1]) shows that some robotic hands designed for research purposes have provided solutions for the domain of prosthesis. However, the actual state of the art shows that the requirements of dexterous manipulation, regarding mechanisms, actuation, and kinematic properties, have not been fulfilled [2]. One important consideration for developing actuation mechanisms concerns the actuation level, robotic hands present in state of the art could be classified mainly into three categories (see Table 1):

1. Under-actuated
2. Fully actuated
3. Over-actuated

Type of actuation is based on the number of actuators used to drive a joint. For instance, a robot having three rotational joints, each one provided with one degree of freedom, could be driven by three actuators (one per joint), in that case, the robot is fully-actuated. When the number of actuators is bigger than the number of joints, the robot is over-actuated. Finally, when the number of actuators is lower than the number of joints, two or more joints must be driven by only one actuator, that case is the underactuated scenario.

Table 1. Summary of robotic hands and its type of actuation

Type of actuation	Name	Source
over-actuated	UTAH	[4–6]
	DextrousHand	[7]
	AwiwiRobotHand	[8]
	TheRobonautHand2	[9,10]
fully-actuated	OkadaHand	[11]
	KeioHand	[12]
	UBHandIV	[13]
	SensorSpeed (OttoBock)	[14]
	ROBIOSS	[15]
under-actuated	i-limb Ultra	[16]
	Université Laval	[17]
	Rutgers Hand	[18]
	i-HY Hand	[19]
	Michelangelo	[20]
	Gifu Hand III	[21]
	MPL Hand	[22]

Regarding functional requirements, Ramirez Arias [3] proposes a study of three critical aspects of the human hand: the kinematics, the functionality, and the dynamics. Concluding that for the development of a prosthetic hand, each finger must:

1. Have an active flexion in the range of $[60, 90]$ degrees in the MCP, PIP, and DIP joints of the finger.
2. Propose an actuation system based on viscoelastic behavior, following the author's proposed Hill-based model (see Figure 1).
3. Perform force in the interval $[4.78\text{N},\ 6.70\text{N}]$.
4. Achieve operating frequency in the interval $[8.89\text{Hz},\ 22.2\text{Hz}]$.

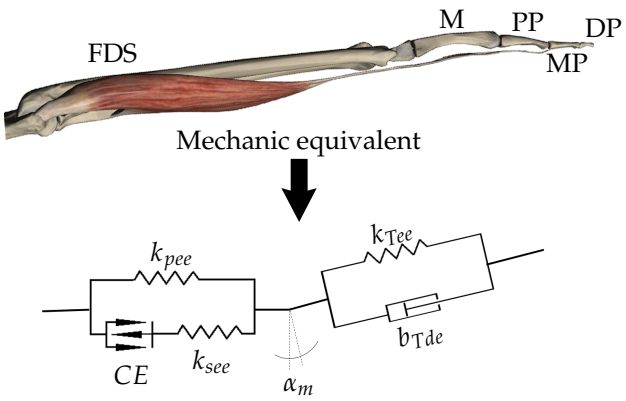

Figure 1. Hill based model proposed by Ramirez Arias [3], to describe the behavior of Flexor Digitorum Superficialis (FDS) muscle, acting over a finger (metacarpus -M-, Proximal phalanges -PP-, Medial phalanges -MP-, and Distal phalanges -DP-).

The Hill-based model, proposed by Ramirez Arias [3], mainly considers two significant variations with respect to classical models: the pennation angle α_m that influences the kinematic and the force during movements, and a parallel damper-spring element representing the tendon to describe the muscle behavior accurately. The complet model presented in Figure 1 is composed by: 1. CE The contractile element, 2. k_{pee} The parallel elastic element of the muscle, 3. k_{see} The muscle's serial elastic element, 4. k_{Tee} The tendon's elastic element, 5. b_{Tde} The tendon's damping element, and 6. α_m The pennation angle. A classic actuation system and a drive mechanism can easily fulfill motion, force,

and frequency requirements. However, a rigid device is not able to mimic the required viscoelastic behavior. Consequently, the first constraint for developing an appropriate mechanism is the inclusion of soft materials in the machinery.

Therefore, in this paper we introduce a biomimetic driving mechanism, aiming to reproduce the viscoelastic behavior of the human muscle, meanwhile satisfying kinematic, dynamic, and static requirements. The device considers the operating principle of the epicyclical mechanism merged with elastic elements.

2. Soft Epicyclical mechanism

According to state of the art developed by Ramirez Arias [3]: 1. the most used drive mechanism is based on tendons, 2. the mass of a prosthetic hand must be under 600g, 3. the number of actuators must be reduced, but the number of DoF must be as high as necessary to perform the prehension, and 4. an electric actuator is a right approach but needs to be complemented with soft elements to achieve the desired behavior. In the following, we introduce the prototype of the so-called robotic finger ProMain-I, which uses a new tendon-driven mechanism (to provide flexibility in the articular joints), and takes into account human hand requirements.

The adduction-abduction of metacarpophalangeal (MCP) joints play an essential role in preparing the hand for grasping. Even that, finger's flexion-extension movements are more significant to perform the hand grasping gesture. Consequently, if the fingers are correctly placed for grasping, adduction-abduction of MCP joints are not required, and the prosthesis can be simplified without impacting prehension ability. Thus, the proposed finger prototype is only endowed with flexion and extension on metacarpophalangeal (MCP), Proximal Interphalangeal (PIP), and Distal Interphalangeal (DIP) joints.

In order to develop the tendon-based ProMain-I finger, an early "alpha" prototype of the robotic finger is introduced. The "alpha" finger prototype is a bio-inspired tendon-driven finger [23–25] composed of three joints: the metacarpophalangeal (MCP), the proximal interphalangeal (PIP) and the distal interphalangeal (DIP). All the joints have one DoF to perform flexion and extension. The finger is controlled by only one actuator, and the drive mechanism uses two tendons for transmitting motion, one for the flexion and one for the extension, as shown in Figure 2. Considering that the tendons are fastened to the motor pulley and the fingertip, the clockwise rotation of the actuator produces the flexion, and the counterclockwise rotation provides the extension.

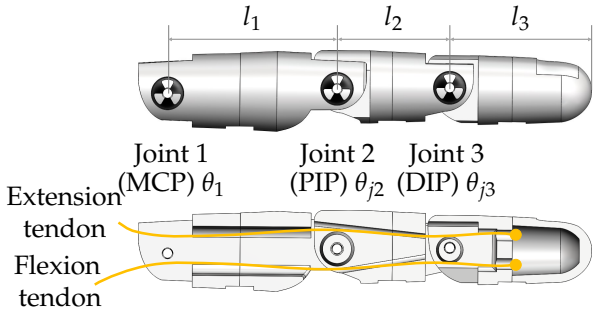

Figure 2. Early "alpha" prototype of the robotic finger.

Due to the under-actuation, the rotation angle of the PIP and DIP joints are linked with the rotation angle of the MCP joint. The relations between joint angles are calculated using experimental measures [24]. As a result, the obtained relations between angles are $\theta_2 = 0.23\theta_1$ and $\theta_3 = 0.72\theta_1$, where θ_1 is the MCP joint angle, θ_2 is the PIP joint angle and θ_3 is the DIP joint angle. Furthermore, the parameters l_1, l_2 and l_3 are the lengths of the proximal, medial and distal phalanges, as shown in Figure 2.

The analysis carried out using experimental data, issued from the "alpha" prototype of the robotic finger, gives us valuable and relevant information for the improvement of the finger's mechanism and

actuation systems, and lets us define the following functional requirements [24,25]: 1. higher stiffness into the MCP joints and 2. a fixed mechanical relation between the proximal and metacarpal joints, and between the distal and metacarpal joints. Those improvements are introduced in the ProMain-I finger prototype.

The new driving mechanism is inspired by the epicyclical gear train, which is typically composed of two gears (one fixed and one mobile) whose centers are attached through a rigid link so-called carrier. So that, the rotation of the carrier creates a revolve of the mobile gear center around the fixed gear. As a result, due to the mechanical link between gears, a rotation is provided on the mobile gear. Furthermore, the rotation amount of the carrier can be different from the rotations of the mobile gear, which is controlled by the gears relation. Figure 3a exemplary shows an epicyclic gear train (whose gears are labeled with white circles to follow relative rotations) in which the carrier has rotate 90° and the mobile gear 150°.

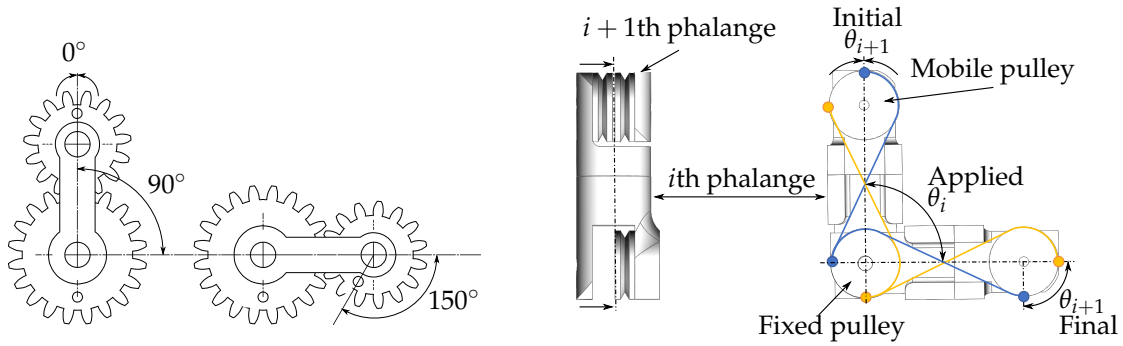

Figure 3. (a) Epicyclical mechanism and (b) Soft epicyclical mechanism.

Consequently, for our driving mechanism, we proposed a soft epicyclical mechanism in which: 1. the finger's phalanges replace the carrier, 2. the gears are replaced by two slotted pulleys, and 3. the mechanical link is guaranteed by two crossed flexible wires, henceforth tendons.

Figure 3b shows the scheme of the driven mechanism, in which blue line represents the tendon that drives clockwise rotation, and the yellow one depicts tendon used to produce counterclockwise rotation; clockwise and counterclockwise rotations are assumed regarding the figure orientation. The ith phalange of the finger begins in a vertical position, then after a rotation, it reaches a horizontal position. The center of the mobile pulley orbits around the fixed pulley, and due to the effect of the tendons, the mobile pulley rotates. As a result, a rotation is produced in the $i+1$th phalange, which is fixed to the mobile pulley. If the mobile pulley gets blocked during rotation, the driving tendon is constrained in tension, so that, the elasticity of the tendon's material depicts the stiffness of the joint.

The proposed soft epicyclic mechanism is used to transmit motion between the MCP joint and the DIP joint, and between the DIP joint and the PIP joint. As a result, two groups of tendons are used; each group is composed of one flexion tendon and one extension tendon. Thus Promain-I hand motion consists in the flexion and extension of the robotic fingers which are placed in the support chassis (60) described above. In the following, we introduce the main components of the ProMain-I hand, see figs. 4a and 4b. The phalanges are the following: 1. proximal (10), which is highlighted in blue color in Figure 4a, 2. medial (20), which is highlighted in yellow color, 3. distal (40), which is highlighted in gray color.

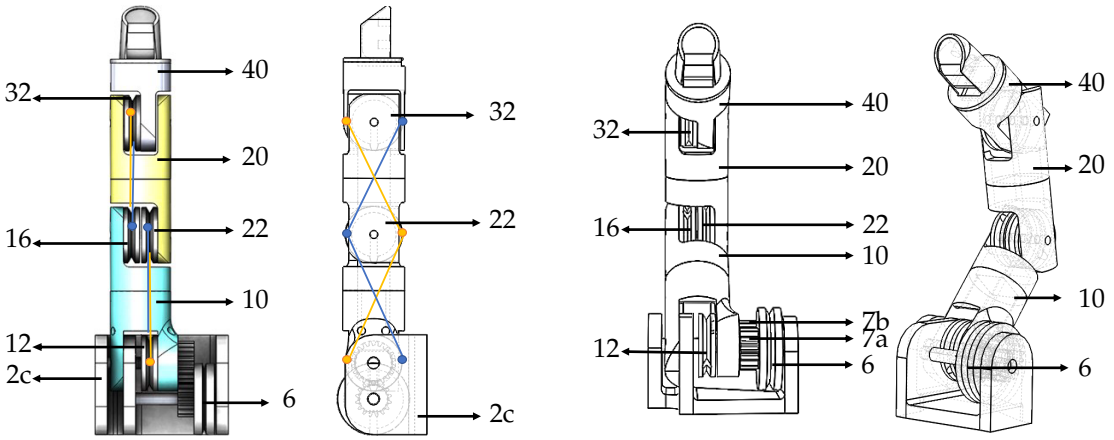

Figure 4. (a) Promain-I finger phalanges description and (b) Promain-I finger main components.

Robotic finger is under-actuated, hence, the movement is transmitted using only one servomotor, which is the active element, it is linked to the MCP joint, through the pulley (6) and the gears (7a and 7b), the gears are used to ensure the rigidity of the proximal phalanx.

Two tendons are crossly placed from pulleys (12) to (22), see Figure 4a, yellow line represents a tendon that executes the flexion of the medial (20) phalange; and blue line illustrates a tendon that executes the extension of medial (20) phalange.

Similarly, pulleys (16) to (32) are linked through two tendons that are crossly attached. Yellow line represents a tendon that executes the flexion of the medial (16) phalanx; and blue line illustrates a tendon that executes the extension of medial (32) phalanx. The motion is executed, following the next steps and conditions:

1. Servomotor is linked to the pulley (6), which transfers the motion to the gear (7a) and (7b).
2. Gear (7b) is attached to the proximal (10) phalanx, therefore the rotation in first phalanx is produced.
3. Pulley (12) is linked with the framework (2c), with this in mind, when the element (10) turns, it causes the rotation of the pulley (22).
4. Pulley (22) is linked to the medial (20) phalanx, thus when the pulley (22) turns, it moves the medial (20) phalanx.
5. Pulley (16) is attached to the phalanx (10), thus, due to the soft epicyclic mechanism, when the pulley (22) turns, it causes a rotation in pulley (32).
6. The pulley (32) is attached to the medial (10) phalanx, so, the rotation of the pulley (32) produces the rotation of the distal phalanx (40).

Two wires or tendons are used to transmit movement from the servomotor to the proximal phalanx. From a qualitative point of view, the elastic behavior of those elements allows us to mimic the human muscle behavior. Furthermore, the same effect is used to reproduce the elastic behavior of human tendons presented in section 1.

The damping element b_{Tde} introduced in section 1 is used to describe more accurately the muscle behavior avoiding undesired oscillations. In this case, considering that no oscillation is present we consider that the element is embedded in the global behavior of the soft epicyclic mechanism. The following fig. 5 shows the equivalence between the proposed mechanism and the Hills-based muscle model.

Peer-reviewed version available at Actuators 2019, 8, 58; doi:10.3390/act8030058

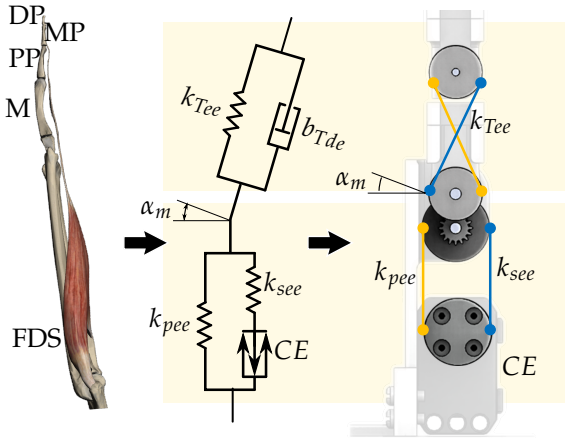

Figure 5. Parallel between soft epicyclic mechanism and the Hills-based muscle model.

As a result, the bio-inspired robotic finger ProMain-I [26], has been developed, tested and manufactured completely in LEME laboratory. The finger has three joints: Metacarpophalangeal (MCP), Proximal interphalangeal (PIP) and distal interphalangeal (DIP). All joints have one degree of freedom (DoF) to perform flexion and extension. Each finger is controlled by only one servo motor XL-320 Dynamixell^{TM}, hence the medial (MP) and distal (DIP) phalanges are driven by the proximal phalanx (PIP) motions. The clockwise rotation of the actuator produces flexion, and the opposite rotation produces extension. The relation between the angles is $\theta_2 = \theta_3 = 0.9\theta_1$, where θ_1 is the MP joint angle, θ_2 is the PIP joint angle and θ_3 is the DIP joint angle. This relation between angles is established manipulating the pulleys ratios and is chosen to mimic the closure of the human hand.

3. Materials and Methods

Considering that the finger prototypes are designed to perform flexion and extension in two dimension, the kinematic is measured using a camera (Canon EOS 600D), pointing single-finger platform shown in Figure 6, to track circular markers placed in finger joints and fingertip. The camera is positioned at 1m from the finger prototype and is adjusted to assure a pixel size of 0.17×0.17mm. The position accuracy (measured comparing several static images with a known value of length) is 0.51mm.

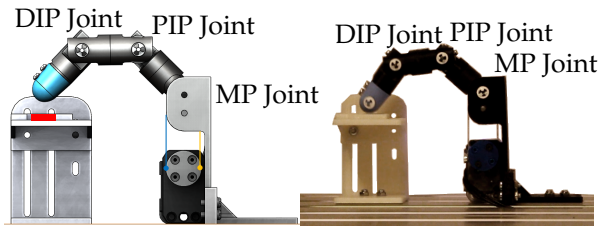

Figure 6. ProMain-I finger test platform.

Images coming from the camera are processed to automatically recognize circular markers. The image analysis follows these Four main steps: 1. Crop image to extract the finger working area, see 7a 2. transform image into a gray scale, see Figure 7b, 3. shift image into a black and white scale, see Figure 7c, 4. detect image edges, see Figure 7d, and 5. apply Hough transform [27] to find the circles positions in the image, see Figure 7e.

Taking into account that digital images are composed by pixels, which are formed by a combination of primary colors organized in three channels red (R), green(G), and blue (B), the gray scale L channel of the image is calculated as the average of the color components. However, both R and G channels are brighter than B, so that, using a simple average the resulting L will appear to be too dark in the red and green areas and too bright in the blue ones. Therefore, a weighted sum of the color components is used to compute the gray scale equivalent as $L = 0.2989R + 0.5870G + 0.1140B$. The

Preprints (www.preprints.org) | NOT PEER-REVIEWED | Posted: 2 April 2019 doi:10.20944/preprints201904.0026.v1

Peer-reviewed version available at Actuators 2019, 8, 58; doi:10.3390/act8030058

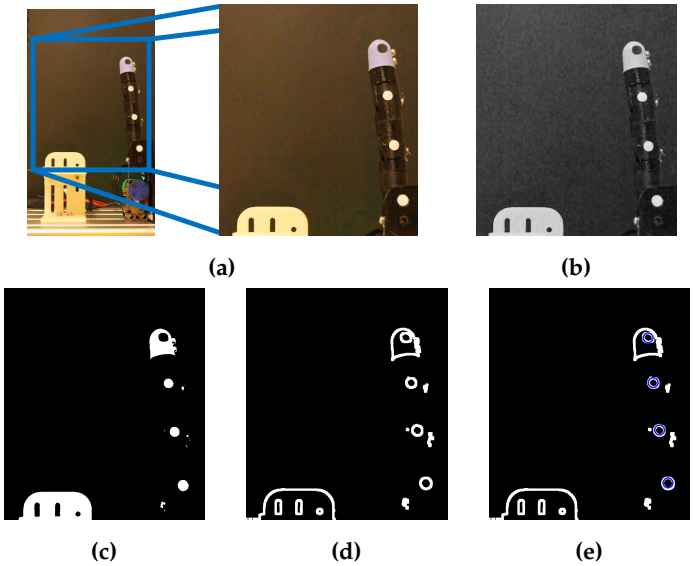

Figure 7. Automatic detection of finger joints an fingertip position: (a) Crop image, (b) Gray scale, (c) Binary image, (d) Image edges, and (e) Hough transform.

coefficients that multiply R, G, and B were originally proposed for encoding analog color television signals and are chosen to avoid information saturation (due to bright) while the image is transformed into black and white scale.

Thereafter, the gray scale image is binarized to obtain a black and white image, which is precessed using a Canny filter [28] to automatically detect image borders; in this step the markers appear to be circles with white borders, see fig. 7d. Finally, the circular Hough's transform is applied to obtain the coordinates of each circle in the image, circles positions correspond to the joint and fingertip coordinates. The image analysis is repeated for the sequence of images stored during flexion and extension tests. Figure 8 shows four sample images of a flexion cycle.

The image analysis delivers the position vectors of the joints, *i.e.* the vectors $\{{}^0P_1^x, {}^0P_1^y, 0\}^T$ for the MCP joint of the finger j, $\{{}^0P_2^x, {}^0P_{j2}^y, 0\}^T$ for the PIP joint and $\{{}^0P_3^x, {}^0P_3^y, 0\}^T$ for the DIP joint. Likewise the vectors $\{{}^0P_f^x, {}^0P_f^y, 0\}$ correspond to the fingertip positions. Considering that the movement is performed in the $xy-$plane, ${}^0P_i^z$ is always zero. The angles are measured as shown in fig. 9, following the DHKK parameterization.

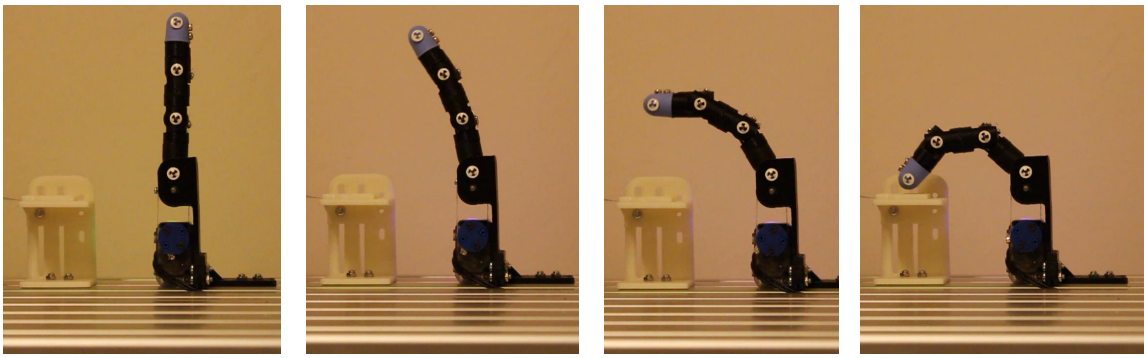

Figure 8. Positions of the robotic finger articulations during flexion

Preprints (www.preprints.org) | NOT PEER-REVIEWED | Posted: 2 April 2019 doi:10.20944/preprints201904.0026.v1

Peer-reviewed version available at Actuators 2019, 8, 58; doi:10.3390/act8030058

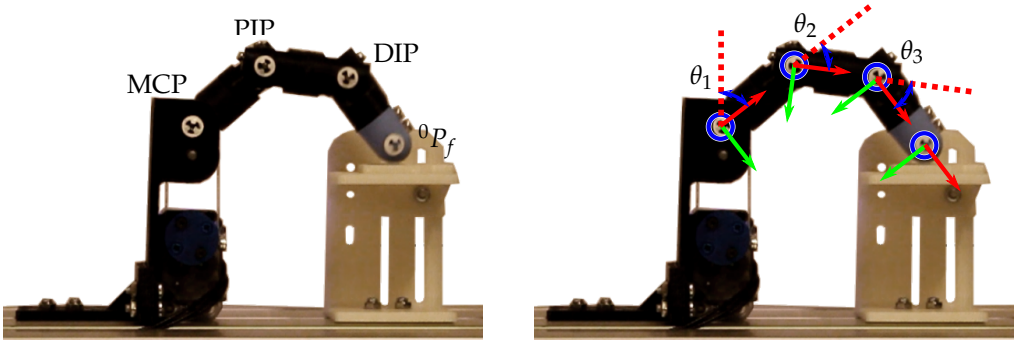

Figure 9. Angles and final position measure

Thereafter, the following three vectors linking joints are defined: 1. vector $\vec{r}_1$ between the MCP and PIP joints, 2. vector $\vec{r}_2$ between the PIP and DIP joints, and 3. vector $\vec{r}_3$ between the DIP joint and fingertip. These vectors are used to calculate rotation angles θ_{ji} as:

$$\theta_i = \arccos\left(\frac{\vec{r}_i \cdot \vec{r}_{i-1}}{\|\vec{r}_i\| \, \|\vec{r}_{i-1}\|}\right) \tag{1}$$

The first angle θ_1 is calculated with respect to a reference positive vertical unitary vector $\vec{r}_0 = 0, 1, 0$, fig. 10 shows the vectors $\vec{r}_i$, the joints and fingertip position, and the location of θ_i.

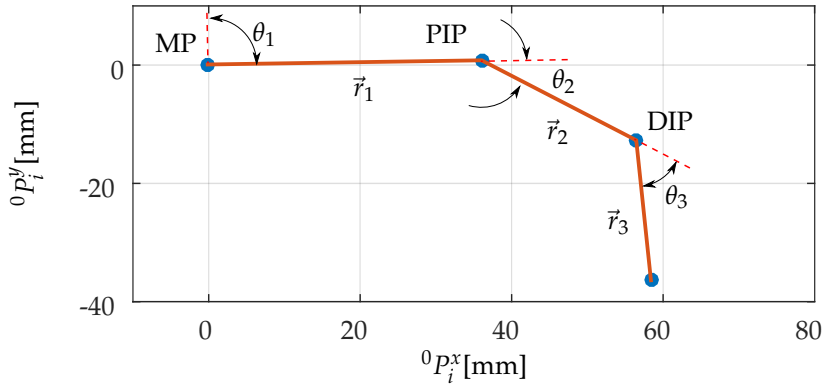

Figure 10. Interpretation of measured kinematic data.

4. Discussion

The experiment carried out with the ProMain-I finger aims to compare the expected rotation relations fixed in the soft epicyclic mechanism and the measured ones to verify the behavior of the finger. We follow the same experimental protocol introduced in section 3. The calculated PIP and DIP joint angles, see Figure 11, shows a under-damped behavior for the PIP and the DIP joints when the finger gets in contact with the platform. This under-damped behavior was expected, considering that the actuation and driving mechanism is not endowed with the damper element. To evaluate the mean absolute error of the PIP and DIP joint angles, we compare the angle value obtained from the kinematic measure with the calculated angle value issued from the relation $\theta_{j2} = \theta_{j3} = 0.9\theta_{j1}$.

Preprints (www.preprints.org) | NOT PEER-REVIEWED | Posted: 2 April 2019 doi:10.20944/preprints201904.0026.v1

Peer-reviewed version available at Actuators 2019, 8, 58; doi:10.3390/act8030058

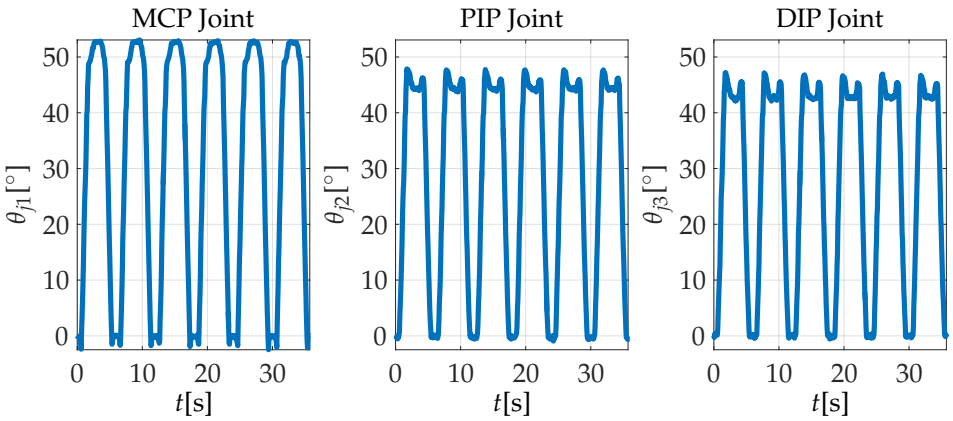

Figure 11. Results of the position tracking of ProMain-I finger.

As a result, we find that the mean absolute error of the angle θ_{j2} is 2.2139°, and the standard deviations is 1.2206°. With respect to the angle θ_{j2} of the DIP joint, the mean absolute error is 2.6235°, and the standard deviations is 1.6370°. Moreover, the probability density function of PIP joint's absolute error presents two peaks values; the first shows a concentration around zero degrees that correspond to the error during free movement, and the second is the error when the finger gets in contact with the object. Likewise, the probability density function of DIP joint's absolute error presents three peaks values the first around zero degrees during free movement and the two others during the contact phase. Both probability density functions are presented in Figures 12a and 12b, in which red lines represent median, cross is mean, a blue box represent the 25% and 75% quartiles and whiskers bound 9% and 91%.

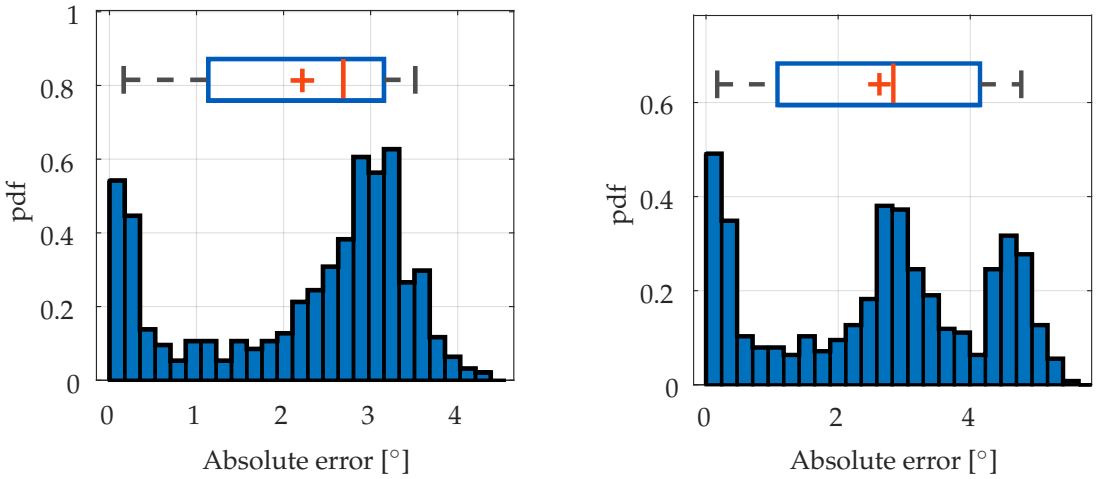

(a) **(b)**

Figure 12. Probability density function of: (a) θ_2 absolute error and (b) θ_3 absolute error.

These error present in the articular joint values θ_2 and θ_3 is the result of the self adaptability of the finger to objects during contact. This effect is the result of the low stiffens of tendons used in the soft epicyclical mechanism.

Furthermore, under some particular conditions, the flexibility of the tendons requires being adapted to grasp objects in a more steady way. Taking into account that the addition of damper element in the tendon adds extra constraints to the soft behavior of the epicyclic mechanism, and considering the advantages of smart materials, we modify the driving mechanism adding a Shape Memory Alloy (SMA) wire in parallel to flexible tendons to control joint stiffness during grasping. As a result, a new soft epicyclic tendon-driven actuation system based on SMA is proposed.

The soft epicyclic tendon-driven actuation system is also based on the proposed hill's muscle model, but the damper is substituted by a SMA wire in order to control the mechanism's stiffness. As can be seen fig. 13, the SMA wire k_{Tce} is place in parallel to the elastic tendon k_{Tee}. During the operation, when the tendon is under a tension F_T a control stimulus (Temperature increment) shift the SMA wire to austenite phase increasing the stiffness to recover the produced strain.

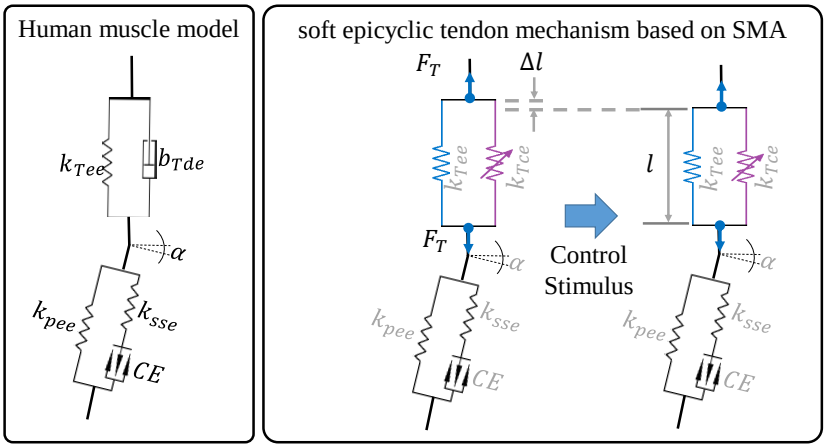

Figure 13. Schematic representation of the soft epicyclic tendon-driven actuation system based on SMA

Preliminary tests have shown that the substitution of the damper element by an SMA wire can reduce or eliminate the overshoot of dependent joint angles. In the following, our research aims to test and validate this theory, through the implementation of a test platform, following the same architecture described in this paper. We expect that the variable stiffness can fulfill damping requirements, helping to mimic the behavior of human muscles.

5. Conclusions

Following the human grasping requirements, a new actuation system, so-called soft epicyclic tendon-based mechanism, is developed to add a soft behavior to the robotic finger joints. The mechanism actuates the soft robotic finger prosthesis ProMain-I, which is under-actuated. The driving mechanism is able to accurately fix the joint angles relations during free movement.

The designed ProMain-I finger is also assessed experimentally with the aim of validating its performance in terms of displacement and force. The PIP and DIP joint angles show a under-damped behavior for the PIP and the DIP joints when the finger gets in contact with the platform where the force sensor is placed. We compare the angle value obtained from the kinematic measure with the calculated angle value issued from fixed transmission relation of the soft epicyclic mechanism. As a result, we find that the mean absolute error of the PIP angle is 2.2139°, and the standard deviations is 1.2206°. With respect to the angle of the DIP joint, the mean absolute error is 2.6235°, and the standard deviations is 1.6370°. This error is coherent with the softness of the driving mechanism.

Finally, we introduce the design of a new version of the soft epicyclic mechanism using an SMA wire in parallel to the flexible tendon for the ProMain robotic finger. This actuation system allows controlling the stiffness of the actuated joints handling the damping effect evidenced during the experiments performed with the ProMain-I finger.

6. Patents

Chaîne articulée comprenant un unique actionneur et ensemble de chaînes articulées associées, patent number FR1656914 [26]: The invention relates to an articulated chain (1), forming in particular all or part of a finger or an arm or a leg or a manipulator, said articulated chain (1) comprising a first member (10), a second member (20) and a flexible seam (30), the first member (10) and the second

member (20) being each attached to the flexible seam (30) which is made of a material having a Shore A hardness of between 0 and 50.

Author Contributions: Conceptualization A.R., J.R.; Data curation P.C., A.R., J.R.; Formal analysis A.R., J.R.; Investigation P.C., A.R., J.R.; Methodology J.R; Validation A.R., J.R.; Writing - original draf P.C., A.R., J.R.; Writing - review and editing P.C., A.R., J.R.

Funding: This research was funded by Universidad Militar Nueva Granada grant number INV-DIS-2961.

Acknowledgments: We would like to acknowledge Université Paris Lumières, and particularly the team of Mécanique des matériaux, des structures et de systèmes at the LEME laboratory for their support.

Conflicts of Interest: The authors declare no conflict of interest..

Abbreviations

The following abbreviations are used in this manuscript:

SMA	Shape Memory Alloy
MCP	Metacarpophalangeal joint
PIP	Proximal Interphalangeal joint
DIP	Distal Interphalangeal joint
FDS	Flexor Digitorum Superficialis muscle
M	metacarpus
PP	Proximal phalanges
MP	Medial phalangesnd
DP	Distal phalanges
CE	The contractile element
k_{pee}	The parallel elastic element of the muscle
k_{see}	The muscle's serial elastic element
k_{Tee}	The tendon's elastic element
b_{Tde}	The tendon's damping element
α_m	The pennation angle

References

1. Zodey, S.; Pradhan, S.K. Matlab Toolbox for Kinematic Analysis and Simulation of Dexterous Robotic Grippers. *Procedia Engineering* **2014**, *97*, 1886–1895. doi:10.1016/j.proeng.2014.12.342.
2. Belter, J.T.; Dollar, A.M. Performance characteristics of anthropomorphic prosthetic hands. Proceedings of IEEE International Conference on Rehabilitation Robotics; IEEE, , 2011; pp. 921–927.
3. Ramirez Arias, J.L. Development of an artificial muscle for a soft robotic hand prosthesis. phdthesis, Univertisé Parias Nanterre, 2016.
4. Narasimhan, S.; Siegel, D.; Hollerbach, J.; Biggers, K.; Gerpheide, G. Implementation of control methodologies on the computational architecture for the Utah/MIT hand. procededings of the International Conference on Robotics and Automation; , 1986; Vol. 3, pp. 1884–1889. doi:10.1109/ROBOT.1986.1087475.
5. Jacobsen, S.C.; Iversen, E.K.; Knutti, D.F.; Johnson, R.T.; Biggers, K.B. Design of the Utah/MIT dextrous hand. proceedings of IEEE International Conference on the Robotics and Automation; , 1986; Vol. 3, pp. 1520–1532.
6. Jacobsen, S.C.; Wood, J.E.; Knutti, D.F.; Biggers, K.B. The UTAH/MIT dextrous hand: Work in progress. *The International Journal of Robotics Research* **1984**, *3*, 21–50.
7. Jacobsen, S.; McCammon, I.; Biggers, K.; Phillips, R. Tactile sensing system design issues in machine manipulation. proceedings of the International Conference on Robotics and Automation, 1987, Vol. 4, pp. 2087–2096. doi:10.1109/ROBOT.1987.1087755.
8. Grebenstein, M. Approaching human performance. PhD thesis, Eidgenössische Technische Hochschule ETH Zürich, 2012.
9. Bridgwater, L.B.; Ihrke, C.A.; Diftler, V.; Abdallah, M.E.; Radford, N.A.; Rogers, J.M.; Yayathi, S.; Askew, R.S.; Linn, D.M. The Robonaut 2 hand - designed to do work with tools. proceedings of the International Conference on Robotics and Automation (ICRA); , 2012; pp. 3425–3430. doi:10.1109/ICRA.2012.6224772.

10. Diftler, V.; Mehling, J.S.; Abdallah, M.E.; Radford, N.A.; Bridgwater, L.B.; Sanders, A.M.; Askew, R.S.; Linn, D.M.; Yamokoski, J.D.; Permenter, F.A.; Hargrave, B.K.; Platt, R.; Savely, R.T.; Ambrose, R.O. Robonaut 2 - The first humanoid robot in space. in procedeedings of the International Conference on Robotics and Automation (ICRA); , 2011; pp. 2178–2183. doi:10.1109/ICRA.2011.5979830.
11. Okada, T. Object-Handling System for Manual Industry. *proceedings of the IEEE Transactions on Systems, Man, and Cybernetics* **1979**, *9*, 79–89. doi:10.1109/TSMC.1979.4310152.
12. Yamano, I.; Maeno, T. Five-fingered Robot Hand using Ultrasonic Motors and Elastic Elements. Proceedings of the 2005 IEEE International Conference on Robotics and Automation; , 2005; pp. 2673–2678. doi:10.1109/ROBOT.2005.1570517.
13. Melchiorri, C.; Palli, G.; Berselli, G.; Vassura, G. Development of the UB Hand IV: Overview of Design Solutions and Enabling Technologies. *IEEE Robotics & Automation Magazine* **2013**, *20*, 72–81. doi:10.1109/MRA.2012.2225471.
14. HealthCare, O. *SensorHand Speed VariPlus Speed*. Deutschland GmbH, Max-Näder-Straße 15, 37115 Duderstadt/Germany, 2013.
15. Mnyusiwalla, H.; Vulliez, P.; Gazeau, J.P.; Zeghloul, S. A New Dexterous Hand Based on Bio-Inspired Finger Design for Inside-Hand Manipulation. *IEEE Transactions on Systems, Man, and Cybernetics: Systems* **2016**, *46*, 809–817. doi:10.1109/TSMC.2015.2468678.
16. touch bionics, 35 Hampden Road Mansfield MA 02048 USA. *i-limb^{TM}ultra Clinician Manual*, 2 ed., 2013.
17. Gosselin, C.; Pelletier, F.; Laliberte, T. An anthropomorphic underactuated robotic hand with 15 dofs and a single actuator. proceedings of the IEEE International Conference on Robotics and Automation; , 2008; pp. 749–754. doi:10.1109/ROBOT.2008.4543295.
18. DeLaurentis, K.J.; Mavroidis, C. Mechanical design of a shape memory alloy actuated prosthetic hand. *Technology and Health Care* **2002**, *10*, 91–106.
19. Odhner, L.U.; Jentoft, L.P.; Claffee, M.R.; Corson, N.; Tenzer, Y.; Ma, R.R.; Buehler, M.; Kohout, R.; Howe, R.D.; Dollar, A.M. A compliant, underactuated hand for robust manipulation. *The International Journal of Robotics Research* **2014**, [http://ijr.sagepub.com/content/early/2014/02/14/0278364913514466.full.pdf+html]. doi:10.1177/0278364913514466.
20. Ottobock, Max-Näder-Straße 15, 37115 Duderstadt/Germany. *The Michelangelo Hand in Practice*.
21. Mouri, T.; Kawasaki, H.; Yoshikawa, K.; Takai, J.; Ito, S. Anthropomorphic robot hand: Gifu hand III. procedings of the International Conference ICCAS; , 2002; pp. 1288–1293.
22. Johannes, M.S.; Bigelow, J.D.; Burck, J.M.; Harshbarger, S.D.; Kozlowski, M.V.; Doren, V.T. An overview of the developmental process for the modular prosthetic limb. *Johns Hopkins APL Technical Digest* **2011**, *30*, 207–216.
23. Ramírez, J.L.; Rubiano, A.; Jouandeau, N.; El korso, M.N.; Gallimard, L.; Polit, O. Hybrid kinematic model applied to the under-actuated robotic hand prosthesis ProMain-I and experimental evaluation. Proceedings of 14th IEEE International Conference on Rehabilitation Robotics (ICORR). IEEE, 2015. doi:10.1109/icorr.2015.7281216.
24. Ramírez, J.L.; Rubiano, A.; Jouandeau, N.; Gallimard, L.; Polit, O., New Trends in Medical and Service Robots. In *New Trends in Medical and Service Robots*; Wenger, P.; Chevallereau, C.; Pisla, D.; Bleuler, H.; Rodić, A., Eds.; Springer International Publishing, 2016; chapter Morphological Optimization of Prosthesis' Finger for Precision Grasping, pp. 249–263. doi:10.1007/978-3-319-30674-2_19.
25. Ramírez, J.L.; Rubiano, A.; Jouandeau, N.; Gallimard, L.; Polit, O., Computational Methods in Applied Sciences. In *Computational Methods in Applied Sciences*; Araujo, A.; Mota Soares, C.A., Eds.; Springer International Publishing, 2016; chapter Artificial Muscles Design Methodology Applied to Robotic Fingers, pp. 209–225. doi:10.1007/978-3-319-44507-6_11.
26. Rubiano, A.; Ramírez, J.L.; Gallimard, L.; Polit, O.; Jouandeau, N. Chaîne articulée comprenant un unique actionneur et ensemble de chaînes articulées associées. France FR1656914, Jul., 2016.
27. Tarsha-Kurdi, F.; Landes, T.; Grussenmeyer, P. Hough-transform and extended ransac algorithms for automatic detection of 3d building roof planes from lidar data. Proceedings of the ISPRS Workshop on Laser Scanning, 2007, Vol. 36, pp. 407–412.
28. Canny, J. A computational approach to edge detection. *IEEE Transactions on pattern analysis and machine intelligence* **1986**, pp. 679–698.

Sample Availability: Information and experimental data are available from the authors.